A Novel Filter Built-in Isolated Bi-directional DC-DC Converter with Split Windings

Shuntaro Inoue, Masanori Ishigaki, Atsuhiro Takahashi, Takahide Sugiyama
Power Electronics & System Lab., Toyota Central R&D Labs., Inc.
41-1, Yokomichi, Nagakute, Aichi, Japan
Email: s-inoue@mosk.tytlabs.co.jp

***Abstract*—A novel filter built-in converter with split windings is presented. Because of its extreme simplicity, flexibility, and efficiency, it has the potential to replace some of the conventional electric power conversion methods used today. The background, design, and operation of the proposed filter built-in converter are discussed in this paper. The proposed converter is derived from a dual active half bridge (DAHB) converter, and it can achieve zero-ripple-current operation and LC low-pass filter function by the split windings and tank capacitors. Due to the zero-ripple-current operation and the LC low-pass filter function, the proposed converter can eliminate or decrease the input and output filters, and with a phase-shift control strategy, all the switches are operated under zero-voltage switching (ZVS) condition. In order to design a power flow control function and a filter function simultaneously, theoretical equations for these functions are derived. Finally, the DAHB and the proposed converter prototypes are constructed for comparison. The results show that the noise in the input port of the proposed prototype is smaller than that of the DAHB prototype by 16 dB (peak), and the proposed approach can achieve a significant improvement in efficiency.**

I. Introduction

Recently, there has been an increase in the number of huge data centers, grid-connected systems for renewable energy, and automotive systems with electric propulsion systems. This has made it necessary to have isolated DC-DC converters, which have properties such as low noise, high efficiency, and high power-density. Dual active half-bridge (DAHB) converter is well known as a half-bridge type dual active bridge (DAB) converter. It has a symmetric structure with phase-shift control, and can control the isolated bidirectional power flow and zero-voltage switching (ZVS) operation for all power switches [1]–[3]. Although the DAHB converter can achieve high efficiency, the filters at the input and output ports for reducing the ripple and harmonics of the input or output are required and the total size of the converter is increased by these filters.

To achieve high efficiency and small size simultaneously, several topologies which can reduce or eliminate the filter components have been proposed, namely interleaved converter [4]–[11], multilevel converter [12]–[14], symmetrical push-pull converter [15]–[17], and isolated Ćuk converter [18]–[20].

Both the interleaved converter [4]–[11] and multilevel converter [12]–[14] can reduce the AC components of the output current at the expense of increasing the complexity of the circuit; however, the input and output currents still have ripple components. Although the symmetrical push-pull converter [15]–[17] can achieve zero-ripple input current, the voltage waveform has ringing during the dead-time period due to the leakage inductance energy, and hence a filter component is still needed at the input port. An isolated Ćuk converter using an integrated magnetic component [18]–[20] can achieve zero-ripple input and output current, and can control bidirectional power flows. However, it has to be operated in the hard-switching condition, and it is difficult to implement unbalancing of leakage inductances in an integrated magnetic component.

In this paper, a new filter built-in DC-DC converter with split windings is proposed. A simple circuit implementation and zero-ripple input and output current can be achieved in ZVS operation by the proposed converter. The proposed converter has the potential to achieve compact and high-efficiency DC-DC conversion by eliminating the input and output filters, due to the zero-ripple operation and the LC low-pass filter function.

II. Proposed Filter Built-in Converter

Fig. 1 shows the circuit diagrams of a conventional dual active half bridge (DAHB) converter with filters and the proposed converter. To clarify the difference between DAHB and the proposed converter, DAHB is represented using split windings in Fig. 1(a). The number of transistors and capacitors used in the proposed converter, as well as the required breakdown voltage of these transistors and capacitors, are the same as that of the DAHB converter.

Fig. 2 shows the theoretical waveforms of the DAHB converter and the proposed converter. The proposed converter can achieve zero-current-ripple operation without input and output filters. Fig. 2(a) shows the theoretical waveforms of the DAHB converter. A ripple current i_{Cin} flows into the input port capacitor C_{in}. The power flow can be controlled by the phase difference ϕ between the primary side and secondary side transistors. Fig. 2(b) shows the theoretical waveforms of the proposed converter. The control strategy for the bidirectional power flow is the same as that of the DAHB converter. The input current i_{in} and output current i_{out} are zero-ripple currents, since the position of the tank capacitor for the current ripple is moved to the inner side of the converter, indicated by $C_{\mathrm{in,tank}}$ and $C_{\mathrm{out,tank}}$. Although the transformer has DC current in each winding, it cancels the DC flux in the

978-1-5386-8330-9/19/$31.00 ©2019 IEEE

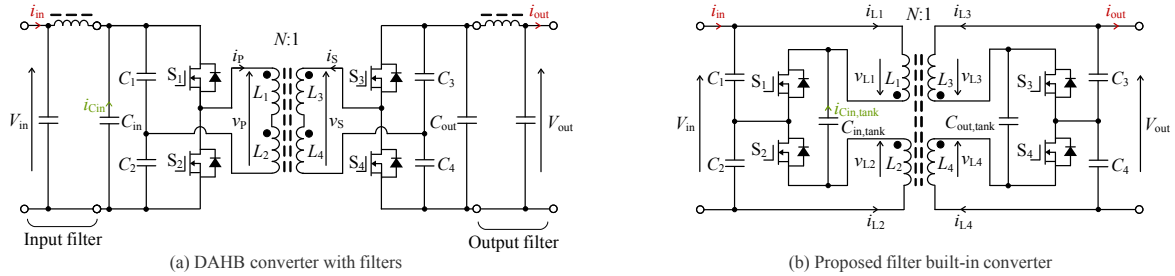

(a) DAHB converter with filters

(b) Proposed filter built-in converter

Fig. 1. Circuit diagrams of the DAHB converter and the proposed converter.

transformer core due to the inverse direction of the windings. The theoretical equation of power flow is written as follows:

$$P_{\mathrm{out,DAHB}} = \frac{NV_{\mathrm{in}}V_{\mathrm{out}}}{4\pi\omega L_{\mathrm{eq,DAHB}}}\phi(\pi - |\phi|) \quad (-\pi \le \phi \le \pi) \quad (1)$$

where $L_{\mathrm{eq,DAHB}}$ is the total leakage inductance of the transformer. When $L_1 = L_2 \equiv L_{\mathrm{P}}$, $L_3 = L_4 \equiv L_{\mathrm{S}}$, $k_{12} \equiv k_{\mathrm{PP}}$, $k_{34} \equiv k_{\mathrm{SS}}$, and $k_{13} = k_{14} = k_{23} = k_{24} \equiv k_{\mathrm{PS}}$ are applied, $L_{\mathrm{eq,DAHB}}$ can be described as follows:

$$L_{\mathrm{eq,DAHB}} = 2(L_{\mathrm{P}} + k_{\mathrm{PP}}L_{\mathrm{P}} + N^2L_{\mathrm{S}} + N^2k_{\mathrm{SS}}L_{\mathrm{S}}) - 8Nk_{\mathrm{PS}}\sqrt{L_{\mathrm{P}}L_{\mathrm{S}}}. \quad (2)$$

Similar to that for the DAHB converter, L_{eq} can be written as follows:

$$L_{\mathrm{eq}} = 2(L_{\mathrm{p}} + k_{\mathrm{pp}}L_{\mathrm{P}} + N^2L_{\mathrm{S}} + N^2k_{\mathrm{SS}}L_{\mathrm{SS}}) - 8Nk_{\mathrm{PS}}\sqrt{L_{\mathrm{P}}L_{\mathrm{S}}}. \quad (3)$$

Thus, the proposed converter has the same leakage inductance as shown in (2) and (3). Using (3), the output power P_{out} of the proposed converter can be written as follows:

$$P_{\mathrm{out}} = \frac{NV_{\mathrm{in}}V_{\mathrm{out}}}{\pi\omega L_{\mathrm{eq}}}\phi(\pi - |\phi|) \quad (-\pi \le \phi \le \pi). \quad (4)$$

Therefore, the proposed converter is capable of controlling a four times larger power range compared to the DAHB, with the same configuration for the transformer windings and the core.

III. Analysis of Built-in Filter Function

The proposed converter has the potential to eliminate the input and output filters in two ways. The first one is zero-current-ripple operations, and the second one is LC low-pass filter function. The two principles of the built-in filter function are presented in this section.

A. Zero-Current-Ripple Operation

When the power flows from the primary side to the secondary side, the ideal waveforms of the DAHB converter and the proposed converter will be as shown in Fig. 2. To derive the ideal waveforms, the following restrictions are assumed.

1) The magnetizing inductance is ignored;
2) All the transistors are ideal switches;
3) The dead time is ignored.

Since the positive half-cycle is symmetrical to the negative half-cycle in the proposed topology, the analysis of the proposed circuit operation will focus only on the positive half-cycle. Under steady-state operation, the proposed converter has three operation stages within the half-cycle as follows:

Subinterval 1 $(0 \le t < t_1)$:
Transistors S_1 and S_4 are in the on-state, and the primary currents i_{L1} and i_{L2} increase. Magnetic energy is charged in the leakage inductance L_{eq} between the primary side windings $(L_1,\ L_2)$ and secondary side windings $(L_3,\ L_4)$.

Subinterval 2 $(t_1 \le t < t_2)$:
The primary currents i_{L1} and i_{L2} become higher than the input currents I_{in} and $-I_{\mathrm{in}}$, respectively. The secondary currents i_{L3} and i_{L4} become lower than the output currents I_{out} and $-I_{\mathrm{out}}$, respectively. Since the currents in the transistors on the primary side and secondary side are represented as $i_{\mathrm{L1}} + i_{\mathrm{L2}}$ and $i_{\mathrm{L3}} + i_{\mathrm{L4}}$, respectively, the directions of currents in the transistors also change from this subinterval.

Subinterval 3 $(t_2 \le t < \pi/\omega)$:
Transistors S_1 and S_3 are in the on-state, and according to the constant current function of the charged magnetic energy in the leakage inductance L_{eq}, electric power flows from V_{in} to V_{out}.

As shown in Fig. 2(b), the proposed converter can achieve zero-ripple operation without input and output filters. In subintervals 1 and 2, the DAHB converter charges the current from the input capacitor C_{in} to a leakage inductance between the primary windings and secondary windings. The charged current causes current-ripples in the input and output ports. As for the proposed converter, the charged current is supplied from a tank capacitor $C_{\mathrm{in,tank}}$. As a result, the proposed converter does not have input and output current ripples.

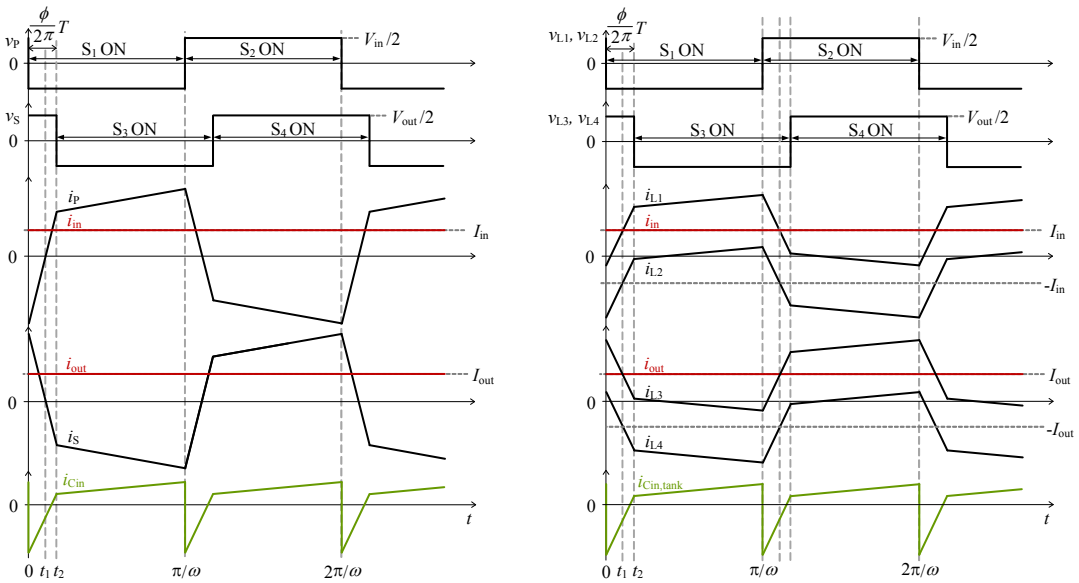

(a) Ideal waveforms of DAHB converter

(b) Ideal waveforms of proposed converter

Fig. 2. Ideal wave forms.

B. LC Low-Pass Filter Function for Switching Noise

Fig. 3 shows the primary side circuit diagrams of the DAHB converter and proposed converter with parasitic components [21]–[23]. C_a and C_b are the sums of the capacitances between the transistors and heat sinks of each power line and case ground. L_a and L_b are the parasitic inductances of the power lines. When the upper side transistor of the DAHB converter turns off, the state of the converter will be in a dead-time mode. The capacitance between the drain and source of the lower side transistor is represented as the output capacitance C_{OSS2} at the lower side transistor. The drain-source voltage v_{DS1} of S_1 changes from 0 to V_in and can be written as follows:

$$v_{\mathrm{DS1}}(t) = k_\mathrm{v} t \ (t > 0) \tag{5}$$

where k_V is the amount of change in the drain-source voltage, which is defined by the physical characteristics of the transistor and the gate resistance. Since v_{DS1} changes like a ramp function, v_{DS2} vibrates, and the voltage $v_{\mathrm{diff}}(= v_{\mathrm{DS1}} + v_{\mathrm{DS2}})$ becomes a noise source.

Fig. 4 shows the differential mode equivalent circuits of the DAHB converter [23] and the proposed converter. The parasitic components L_a, L_b, C_a, and C_b are approximated to zero, since their influences on the differential mode current $(i_\mathrm{a} - i_\mathrm{b})/2$ are considerably small. Unlike the DAHB converter, the proposed converter has leakage inductances $(1-k_{12})L_1 + (1-k_{12})L_2$ between noise source $v_{\mathrm{diff,in}}$ and port voltage $v_{\mathrm{diff,out}}$. Therefore, the proposed converter can filter the differential mode current generated from the noise source voltage v_{diff} by using the LC low-pass filter composed of $(1-k_{12})L_1$, $(1-k_{12})L_2$, C_1, and C_2.

Fig. 5 shows the common mode equivalent circuits of the DAHB converter [23] and the proposed converter, where the common mode noise voltage source v_{com} is derived from a bridge circuit composed of L_a, L_b, C_a, and C_b as shown in Fig. 6, where Z_R is a common mode impedance connected to v_{com}. The common mode currents are generated by the unbalances of the bridge circuits. Compared to the DAHB converter, the proposed converter has an integrated inductance $(1+k_{12})L_1$ between $v_{\mathrm{com,in}}$ and $v_{\mathrm{com,out}}$. By designing the amount of $(1+k_{12})L_1$, C_{F1}, and C_{F2} appropriately, the inductance of the power converter can be used as a common mode low-pass filter.

C. Theoretical equation of filter functions

The theoretical equations of the filter functions for each current mode are written as follows:

1) Differential current mode:

The transfer function $v_{\mathrm{diff,out}}/v_{\mathrm{diff,in}}$ of the differential filter function is written as follows:

$$\frac{v_{\mathrm{diff,out}}}{v_{\mathrm{diff,in}}} = \frac{\frac{1}{L_{\mathrm{diff}}C_{\mathrm{diff}}}}{s^2 + \frac{R_{\mathrm{diff}}}{L_{\mathrm{diff}}}s + \frac{1}{L_{\mathrm{diff}}C_{\mathrm{diff}}}} \tag{6}$$

where $v_{\mathrm{diff,in}}$ is the noise voltage source and $v_{\mathrm{diff,out}}$ is the port voltage for the differential mode. L_{diff} and C_{diff} can be defined as follows:

$$L_{\mathrm{diff}} = (1-k_{12})L_1 + (1-k_{12})L_2 \tag{7}$$

$$C_{\mathrm{diff}} = \frac{C_1 C_2}{C_1 + C_2} \tag{8}$$

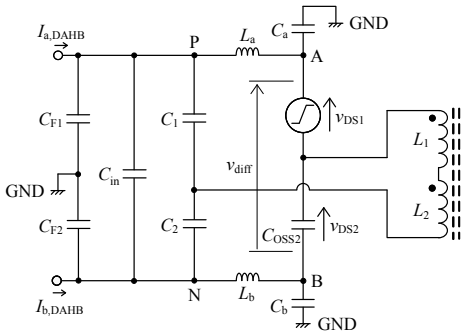

(a) Primary side of DAHB with parastic elements

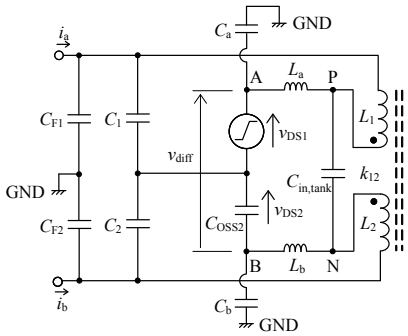

(b) Primary side of proposed topology with parastic elements

Fig. 3. Primary side circuits with parastic components.

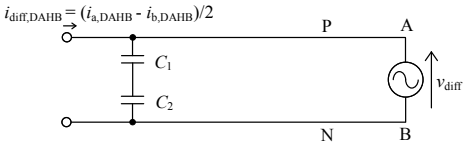

(a) DAHB

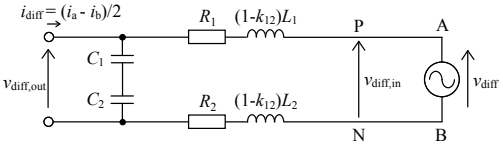

(b) Proposed topology

Fig. 4. Equivalent circuit for differential current mode of each topology

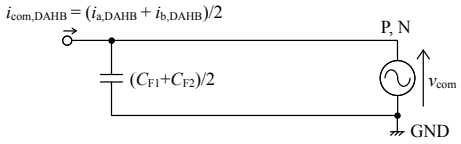

(a) DAHB

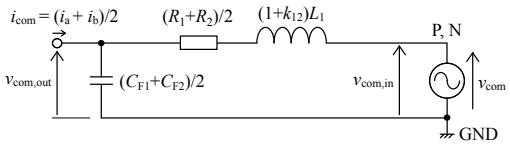

(b) Proposed topology

Fig. 5. Equivalent circuit for common current mode of each topology

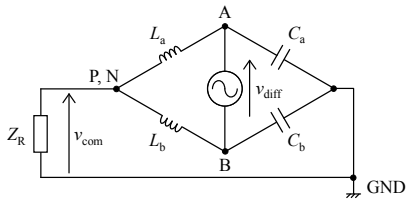

Fig. 6. Conversion from differential mode voltage noise source $v_{\rm diff}$ into commom mode voltage noise source $v_{\rm com}$.

When the series resistance of L_1 and L_2 are assumed as R_1 and R_2, respectively, $R_{\rm diff}$ can be written as follows:

$$R_{\rm diff} = R_1 + R_2 \tag{9}$$

When the impedance of $R_{\rm diff}$ is considerably smaller than that of $L_{\rm diff}$ and $C_{\rm diff}$, the cut-off frequency for the differential mode can be written as follows:

$$f_{\rm diff} = \frac{1}{2\pi\sqrt{L_{\rm diff}C_{\rm diff}}} \tag{10}$$

2) Common current mode:

The transfer function $v_{\rm com,out}/v_{\rm com,in}$ is written as follows:

$$\frac{v_{\rm com,out}}{v_{\rm com,in}} = \frac{\frac{1}{L_{\rm com}C_{\rm com}}}{s^2 + \frac{R_{\rm com}}{L_{\rm com}}s + \frac{1}{L_{\rm com}C_{\rm com}}} \tag{11}$$

where $v_{\rm com,in}$ is the noise voltage source and $v_{\rm com,out}$ is the port voltage for the common mode. $L_{\rm com}$, $C_{\rm com}$, and $R_{\rm com}$ can be written as follows:

$$L_{\rm com} = (1 + k_{\rm PP})L_{\rm P} \tag{12}$$

$$C_{\rm com} = \frac{C_{\rm F1} + C_{\rm F2}}{2} \tag{13}$$

$$R_{\rm com} = \frac{R_1 + R_2}{2} \tag{14}$$

When the impedance of $R_{\rm com}$ is considerably smaller than that of $L_{\rm com}$ and $C_{\rm com}$, the cut-off frequency for the common

mode can be written as follows:

$$f_{\mathrm{com}} = \frac{1}{2\pi\sqrt{L_{\mathrm{com}}C_{\mathrm{com}}}} \tag{15}$$

D. Zero-voltage switching analysis

Although the proposed converter has DC-bias in the transformer windings, the currents in the transistors have no DC-bias because the transistor currents are the sums of the two currents in the windings on the same side. Hence, for analysis of the ZVS region, the input current $i(\phi,t)$ is defined as $i(\phi,t) = i_{\mathrm{L1}}(\phi,t) + i_{\mathrm{L2}}(\phi,t)$. In each subinterval, the input current $i(\phi,t)$ is depicted as shown in Fig. 7, and is written as follows:

$$i(\phi,t) = -I_{\mathrm{P2}} + \frac{V_{\mathrm{in}}+NV_{\mathrm{out}}}{L_{\mathrm{eq}}}t, \left(0 \le t < \frac{\phi}{\omega}\right) \tag{16}$$

$$i(\phi,t) = I_{\mathrm{P1}} + \frac{V_{\mathrm{in}}-NV_{\mathrm{out}}}{L_{\mathrm{eq}}}t, \quad \left(\frac{\phi}{\omega} \le t < \frac{\pi}{\omega}\right) \tag{17}$$

$$i(\phi,t) = I_{\mathrm{P2}} - \frac{V_{\mathrm{in}}+NV_{\mathrm{out}}}{L_{\mathrm{eq}}}t, \quad \left(\frac{\pi}{\omega} \le t < \frac{\pi+\phi}{\omega}\right) \tag{18}$$

$$i(\phi,t) = -I_{\mathrm{P1}} - \frac{V_{\mathrm{in}}-NV_{\mathrm{out}}}{L_{\mathrm{eq}}}t, \left(\frac{\pi+\phi}{\omega} \le t < \frac{2\pi}{\omega}\right) \tag{19}$$

where I_{P1} and I_{P2} are defined as the currents at $t = \phi/\omega$ and $t = \pi/\omega$, respectively.

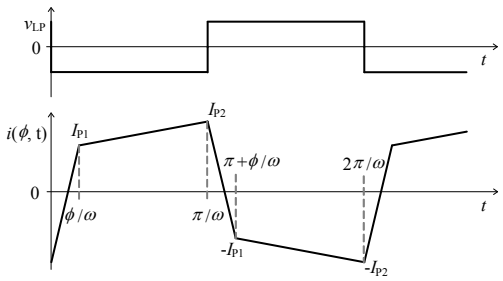

Fig. 7. An example of primary voltage and current waveforms.

If I_{P1} is positive, the output side transistors S_3 and S_4 achieve ZVS. Similarly, if I_{P2} is positive, the input side transistors S_1 and S_2 achieve ZVS. Hence, the ZVS requirements can be written as follows:

$$I_{\mathrm{P1}} = \frac{(\phi-\pi)V_{\mathrm{in}} + 2\phi NV_{\mathrm{out}}}{2\omega L_{\mathrm{eq}}} > 0 \tag{20}$$

$$I_{\mathrm{P2}} = \frac{(\pi-\phi)V_{\mathrm{in}} - 2(\pi-2\phi)NV_{\mathrm{out}}}{2\omega L_{\mathrm{eq}}} > 0 \tag{21}$$

By rearranging (20) and (21), the ZVS boundaries are represented as follows:

$$\phi = \frac{\pi}{2}\left(1 - \frac{NV_{\mathrm{out}}}{V_{\mathrm{in}}}\right) \tag{22}$$

$$\phi = \frac{\pi}{2}\left(1 - \frac{V_{\mathrm{in}}}{NV_{\mathrm{out}}}\right) \tag{23}$$

When N = 1.0 and $V_{\mathrm{out}}/V_{\mathrm{in}} < 1.0$, the ZVS boundary is depicted by (22), and when N = 1.0 and $V_{\mathrm{out}}/V_{\mathrm{in}} \ge 1.0$, the ZVS boundary is depicted by (23).

Fig. 8 shows the ZVS regions when the winding ratio N is changed in three patterns. Since the ZVS boundary equation is changed according to the voltage ratio $V_{\mathrm{out}}/V_{\mathrm{in}}$, the regions are divided into three areas as follows:

(A): The input side transistors S_1 and S_2 are operated in the hard-switching mode, and the output transistors S_3 and S_4 are operated in the ZVS mode.

(B): All the transistors can achieve ZVS.

(C): The input side transistors S_1 and S_2 are operated in the ZVS mode, and the output transistors S_3 and S_4 are operated in the hard-switching mode.

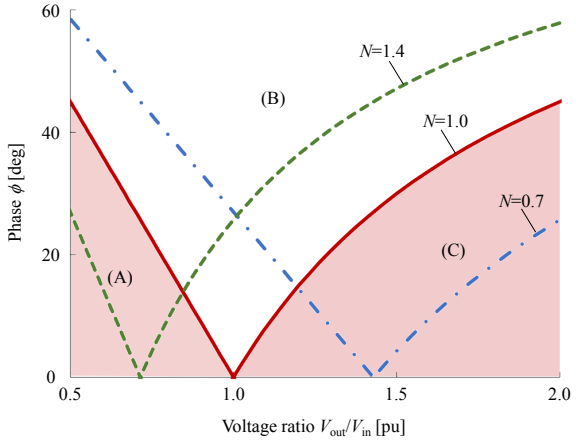

Fig. 8. ZVS region of the proposed converter.

E. Theoretical maximum magnetic density

The magnetic density of the DAHB converter $B_{0-\mathrm{P,DAHB}}$ and that of the proposed converter $B_{0-\mathrm{P}}$ are written as follows:

$$B_{0-\mathrm{P,DAHB}} = \frac{\pi V_{\mathrm{in}}}{8\omega N_{\mathrm{L1'}}A} \tag{24}$$

$$B_{0-\mathrm{P}} = \frac{\pi V_{\mathrm{in}}}{4\omega(N_{\mathrm{L1}} + N_{\mathrm{L2}})A} \tag{25}$$

where $N_{\mathrm{L1}'}$, N_{L1}, and N_{L2} are the turn numbers of L_1', L_1, and L_2, respectively, and A is the effective cross section of the magnetic core.

IV. Experimental system

In order to verify the operational principle of the proposed converter and compare it with the DAHB converter, prototypes of the proposed converter and DAHB converter were implemented as shown in Fig. 9.

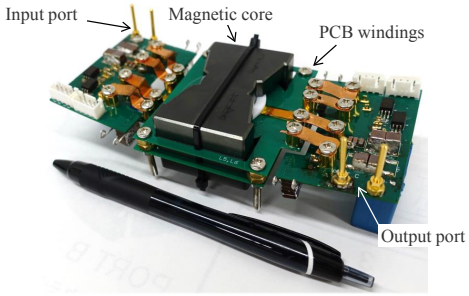

Fig. 9. Overview of the proposed converter prototype

The experimental setup is shown in Fig. 10. The electric voltage sources and electric loads are connected to the input ports and output ports of both converters, respectively. The switching frequency is 200 kHz, and the input voltage V_{in} and output voltage V_{out} are set to 48 V. The winding ratios of the transformers are set to 1:1.

Using (24) and (25), the magnetic components of the DAHB converter and the proposed converter were designed. The turn numbers of L_1', L_2', L_1, L_2, L_3, and L_4 were set to 4. In this condition, the total winding volume, magnetic core volume, and maximum magnetic flux density are the same for the two converters.

For fair comparison between the DAHB converter and the proposed converter, both the converters use the same number of PCB windings (4 turns, copper thickness: 175 μm). DAHB uses two boards in parallel for L_1' and L_2'. The proposed converter uses one board for L_1, L_2, L_3, and L_4.

Table I summarizes the parameters of the electrical components in the DAHB converter and the proposed converter. To compare the current ripples under the same conditions, the same values of capacitance are implemented in each part of the two converters, as shown in Table I. To measure the common currents, midpoint M is set between C_{F1} and C_{F2} in both the DAHB converter and the proposed converter. The midpoint M is connected to the heat sink of the primary side for S_1 and S_2 to simulate common mode environment as shown in Fig. 3.

TABLE I
Basic parameters of the DAHB converter and the proposed converter

Description	Property	
Switching frequency	f_{sw}	200 kHz
Rated power	$P_{\mathrm{out.max}}$	500 W
Rated DC Voltage	$V_{\mathrm{in}},\ V_{\mathrm{out}}$	48 V, 48 V
Magnetic core	-	Ferrite PC9PQ60/42 (TDK)
Core gap	-	0.0 mm
Si MOSFET	$\mathrm{S}_1,\ \mathrm{S}_2$ $\mathrm{S}_3,\ \mathrm{S}_4$	IRFH7185TRPBF (Infineon)
DC capacitor	$C_1,\ C_2$ $C_3,\ C_4$	100 μF
DC capacitor	$C_{\mathrm{in}}, C_{\mathrm{out}}$	30 μF
DC capacitor	$C_{\mathrm{in,tank}}$, $C_{\mathrm{out,tank}}$	30 μF
DC capacitor	$C_{\mathrm{F1}},\ C_{\mathrm{F2}}$	1 nF
Turn number of primary side	$N_{\mathrm{L1}'}$, $N_{\mathrm{L1}},\ N_{\mathrm{L2}}$	4, 4, 4
Turn number of secondary side	$N_{\mathrm{L2}'}$, $N_{\mathrm{L3}},\ N_{\mathrm{L4}}$	4, 4, 4
Equivalent leakage inductance	0.29 μH, 1.14 μH	$L_{\mathrm{eq,DAHB}}$, L_{eq}
Self inductance of primary side	L_1', $L_1,\ L_2$	322.4 μH, 320.0 μH, 320.1 μH
Self inductance of secondary side	L_2', $L_3,\ L_4$	322.3 μH, 319.9 μH, 320.1 μH

V. Experimental results

Fig. 11 shows the operational waveforms of the DAHB converter and the proposed converter when the output power is 500 W. Fig. 11(a) shows the transformer currents. The leakage inductance L_{eq} calculated from the transformer current is 1.21 μH, which corresponds with the value estimated using the LCR meter (1.14 μH). Fig. 11(b) shows a comparison of the input currents in the differential mode, where $i_{\mathrm{diff,DAHB}}$ and i_{diff} are the differential mode current defined by $i_{\mathrm{diff,DAHB}} = (i_{\mathrm{a,DAHB}} - i_{\mathrm{b,DAHB}})/2$ and $i_{\mathrm{diff}} = (i_{\mathrm{a}} - i_{\mathrm{b}})/2$, respectively. The input current of the proposed converter was found to be smoother than that of the DAHB converter because of the zero-current-ripple operation.

Fig. 12 shows the result of the spectrum analysis for the differential mode currents. At the frequency where DAHB has the peak amplitude, the amplitude of the proposed converter is smaller than that of the DAHB converter by 16 dB.

The common mode input current was also evaluated, and the peak amplitude of the proposed converter is smaller than that of DAHB converter by 2 dB, as shown in Fig. 13. Since there is only switching noise in common mode, the result means that the amplitude is decreased by LC low-pass filter function.

Fig. 14 shows the efficiency curves of the proposed converter and the two types of DAHB converters. The bigger DAHB is designed using a transformer core of the same size as that of the proposed prototype. Due to the filter components, its overall size is bigger than that of the proposed prototype by 50 cc. The assumed filters consist of two common mode chokes (Self inductance: 320 μH, Leakage inductance: 1.2 μH) and two capacitors (50 μF). The downsized DAHB is designed

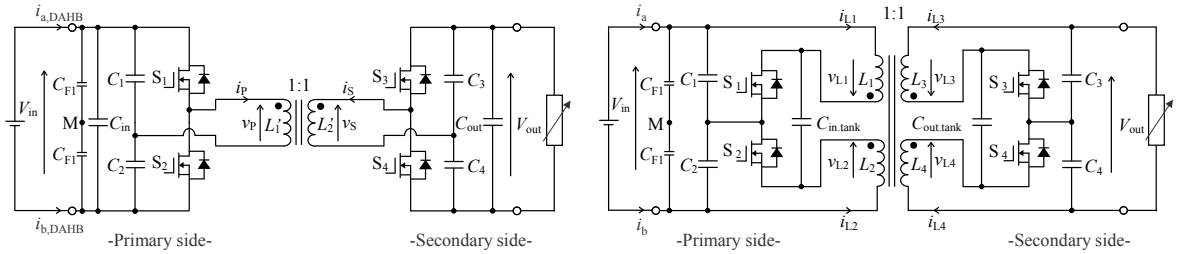

(a) DAHB converter without filters (b) Proposed filter built-in converter

Fig. 10. Experimental setup

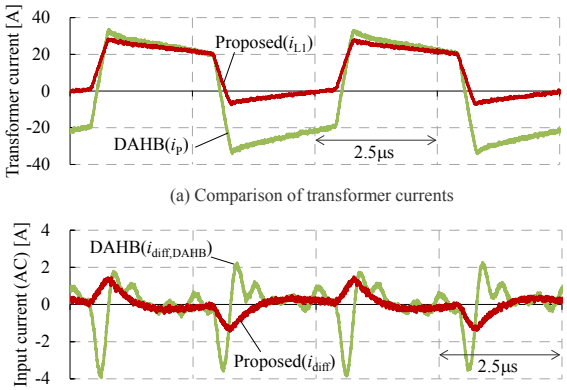

(a) Comparison of transformer currents

(b) Comparison of input currents (AC components)

Fig. 11. Experimental waveforms

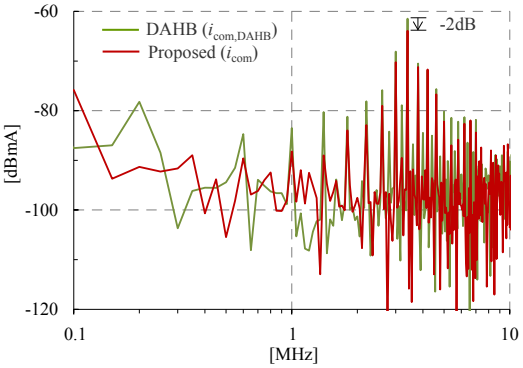

Fig. 13. Comparison of noise in common mode

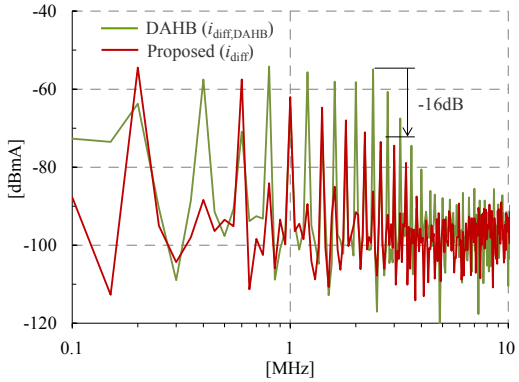

Fig. 12. Comparison of noise in differential mode

using a transformer core of smaller size. The total size of the downsized DAHB is reduced by the narrowed widths of the transformer windings and core window. The triangle mark and square mark indicate the efficiencies of the DAHB converter including the estimated filter conduction loss and downsized effect. In the estimation, the turn number and width of windings for the input and output filters are the same as those of the proposed circuit.

At 500 W, the efficiency of the proposed prototype is higher than that of the downsized DAHB converter by 2% because the proposed converter integrates the filter components and can offer wider windings than the downsized DAHB. Therefore, if the proposed converter is designed with the same size as that of the DAHB converter, including the filter size, the proposed converter can improve the efficiency because the transformer size can be increased compared to the DAHB converter.

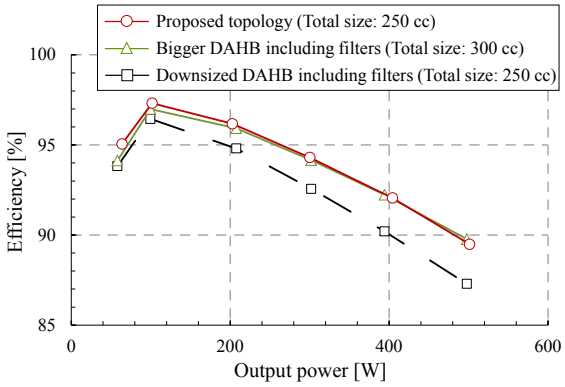

Fig. 14. Experimental results about efficiency

VI. Conclusion

In this paper, a filter built-in bidirectional isolated DC-DC converter is proposed, and the prototypes of the proposed converter and the conventional DAHB converter were implemented and evaluated. The proposed converter has split windings and tank capacitors, and the number of capacitors and transistors as well as the breakdown voltage and current required by the capacitor and transistor are the same as that in the DAHB converter. Furthermore, the power flow controlling strategy is also the same as DAHB, hence the proposed converter can achieve ZVS operation. Using the prototypes, an improvement in the noise at the input port was achieved in both the differential mode and common mode. With the built-in filter function, improvement in size and efficiency can be achieved.

References

[1] R. W. De Doncker, D. M. Divan, and M. H. Kheraluwala, "A three-phase soft-switched high-power-density dc/dc converter for high-power applications," *IEEE transactions on industry applications*, vol. 27, no. 1, pp. 63–73, 1991.

[2] S. Inoue and H. Akagi, "A bidirectional dc–dc converter for an energy storage system with galvanic isolation," *IEEE Transactions on Power Electronics*, vol. 22, no. 6, pp. 2299–2306, 2007.

[3] F. Krismer and J. W. Kolar, "Accurate power loss model derivation of a high-current dual active bridge converter for an automotive application," *IEEE Transactions on Industrial Electronics*, vol. 57, no. 3, pp. 881–891, 2010.

[4] K. K. Hedel, "High-density avionic power supply," *IEEE Transactions on Aerospace and Electronic Systems*, no. 5, pp. 615–619, 1980.

[5] T. Qian and B. Lehman, "Dual interleaved active-clamp forward with automatic charge balance regulation for high input voltage application," *IEEE transactions on power electronics*, vol. 23, no. 1, pp. 38–44, 2008.

[6] L.-P. Wong, Y.-S. Lee, M. H. Chow, and D. K.-W. Cheng, "A four-phase forward converter using an integrated transformer," *IEEE Transactions on Industrial Electronics*, vol. 55, no. 2, pp. 817–831, 2008.

[7] M. T. Zhang, M. M. Jovanovic, and F. C. Lee, "Analysis and evaluation of interleaving techniques in forward converters," *IEEE Transactions on Power Electronics*, vol. 13, no. 4, pp. 690–698, 1998.

[8] B. Tamyurek and B. Kirimer, "An interleaved high-power flyback inverter for photovoltaic applications," *IEEE transactions on Power Electronics*, vol. 30, no. 6, pp. 3228–3241, 2015.

[9] J. C. Liu, N. Poon, B. M. Pong, and C. Tse, "Low output ripple dc-dc converter based on an overlapping dual asymmetric half-bridge topology," *IEEE transactions on power electronics*, 2007.

[10] X. Wu, W. Lu, J. Zhang, and Z. Qian, "Extra wide input voltage range and high efficiency dc-dc converter using hybrid modulation," in *Industry Applications Conference, 2006. 41st IAS Annual Meeting. Conference Record of the 2006 IEEE*, vol. 2. IEEE, 2006, pp. 588–594.

[11] X. Wang, F. Tian, and I. Batarseh, "High efficiency parallel post regulator for wide range input dc–dc converter," *IEEE Transactions on Power Electronics*, vol. 23, no. 2, pp. 852–858, 2008.

[12] F. Deng and Z. Chen, "Control of improved full-bridge three-level dc/dc converter for wind turbines in a dc grid," *IEEE Trans. Power Electron.*, vol. 28, no. 1, pp. 314–324, 2013.

[13] L. F. Costa, S. A. Mussa, and I. Barbi, "Multilevel buck/boost-type dc–dc converter for high-power and high-voltage application," *IEEE Transactions on Industry Applications*, vol. 50, no. 6, pp. 3931–3942, 2014.

[14] Z. Guo, K. Sun, and D. Sha, "Improved zvs three-level dc–dc converter with reduced circulating loss," *IEEE Transactions on Power Electronics*, vol. 31, no. 9, pp. 6394–6404, 2016.

[15] R.-S. Lai, K. Ngo, and J. Watson, "Steady-state analysis of the symmetrical push-pull power converter employing a matrix transformer," *IEEE transactions on power electronics*, vol. 7, no. 1, pp. 44–53, 1992.

[16] C.-S. Leu and J.-B. Hwang, "A built-in-input filter forward converter," in *Power Electronics Specialists Conference, PESC'94 Record., 25th Annual IEEE*, vol. 2. IEEE, 1994, pp. 917–921.

[17] P. Xu, M. Ye, P.-L. Wong, and F. C. Lee, "Design of 48 v voltage regulator modules with a novel integrated magnetics," *IEEE Transactions on Power Electronics*, vol. 17, no. 6, pp. 990–998, 2002.

[18] S. Cuk, "A new zero-ripple switching dc-to-dc converter and integrated magnetics," *IEEE Transactions on Magnetics*, vol. 19, no. 2, pp. 57–75, 1983.

[19] S. Cuk and R. Middlebrook, "Advances in switched-mode power conversion part i," *IEEE Transactions on Industrial Electronics*, no. 1, pp. 10–19, 1983.

[20] S. Cuk and R. Middlebrook, "Advances in switched-mode power conversion part ii," *IEEE Transactions on Industrial Electronics*, no. 1, pp. 19–29, 1983.

[21] M. Shoyama, G. Li, and T. Ninomiya, "Balanced switching converter to reduce common-mode conducted noise," *IEEE Transactions on Industrial Electronics*, vol. 50, no. 6, pp. 1095–1099, 2003.

[22] P. Kong, S. Wang, F. C. Lee, and Z. Wang, "Reducing common-mode noise in two-switch forward converter," *IEEE Transactions on Power Electronics*, vol. 26, no. 5, pp. 1522–1533, 2011.

[23] A. Takahashi, H. Tsukada, T. Kojima, Y. Hattori, T. Funaki, and O. Wada, "Analysis of commom-mode noise generation mechanism in fm radio band caused by dc-dc converter," R&D Review of Toyota CRDL, Tech. Rep., 2017.